

Unobtrusive Respiratory Rate Detection Within Homecare Scenarios

Bjoern-Helge Busch and Ralph Welge

Abstract Against the background of Ambient Assisted Living, this article proposes a new kind of unobtrusive, non-stigmatizing and continuous acquisition of vital signs as respiratory rate and related features on the basis of ultra-wide-band radar sensing. Through the runtime analysis of the reflection data, surrogating mechanical signals e.g. the excursion of the thorax are detected and linked with physiological values like the breathing rate. After a brief introduction to the application context including an explanation of specific user demands and restrictions of current solutions of the telemedicine, physical fundamentals of measurement and the utilized electronics, the applied principles of spatial and temporal data mining are described. Finally, experiments including real measurements with the subsequent discussion of the measurement results provide an outlook to the capabilities of our approach and grant information about open issues and the steps in research.

1 Introduction

Due to the demographic trend in most of the highly industrialized countries, in particular in Germany, the scientific area of *Ambient Assisted Living*, abbreviated by the acronym AAL, gained much more importance in recent years and was expedited by a couple of research projects funded by the BMBF, a German governmental institution for research and education. AAL comprehends technical

B.-H. Busch (✉) · R. Welge
Leuphana University Lueneburg, Institute VauST,
Volgershall 1, 21339 Lueneburg, Germany
e-mail: bhbusch@leuphana.de

R. Welge
e-mail: welge@leuphana.de

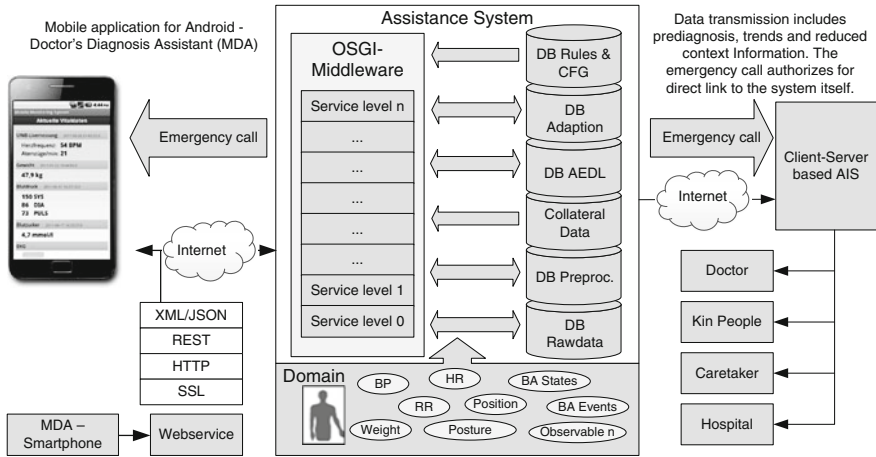


Fig. 1 Concept of an AAL-infrastructure [1]

solutions and concepts for the unobtrusive support of elderly people in their familiar environment. Obviously, this approach implies the usage of ambient intelligence technologies for the collection of user data and the initiation of domain interventions (e.g. emergency detection or domain regulations). Many AAL-research projects deal with the development of human centered assistance systems, including the development of agents for early emergency detection, preventive diagnosis, energy awareness, compliance control and medicine management (refer to Fig. 1). The context aware analysis of certain living patterns covering snap shots of health parameters requires a robust and reliable acquisition of these values—the main objective of further considerations.

1.1 Limitations of the Telemedicine for AAL-Domains

Usually, in home care domains, established components of the telemedicine are applied. In our approach for an assistance system, we utilize telemedical solutions for the acquisition of weight, heart rate, blood oxygen, blood glucose, respiratory rate through nasal prongs et cetera equipped with a Bluetooth interface. However, these devices reveal a lot of disadvantages considering usability, significance and validity of gathered raw data and questions of ethics as listed below.

- The patient has to use telemedical devices autonomously on his own. In accordance to anamnesis and latest therapy recommendations, this has to be done at determined instants of time. Otherwise, the raw data is not trustworthy or out of sync with the aim of acquisition. The extracted information may be diagnostically less conclusive.

- The usage of telemedical devices is often inconvenient. Further, many body attached sensor networks (BSN) restrict the user in their autonomy, agility and mobility. Chest straps are impractical for long-term surveillance.
- The usage of BSNs is not only a question of comfort but also a factor of stigmatization. Therefore, visible measurement of vital signs should be avoided in home care scenarios.
- Imaging techniques based on the evaluation of cameras for the identification of position, posture, activity, agility and emotional shape are inappropriate. The user rejects, or often only accepts them with reservations because this approach procures an impression of observation.

Regarding to these mentioned deficits, it is recommended to avoid camera-based systems or BSNs. Therefore, we prefer the use of a UWB-sensor and concentrate first of all on the most significant vital parameter we can observe: the respiration rate.

1.2 Main Target: Identification of Respiratory Rate

Two main aspects are in the focus of interest—the determination of the physical shape of a human and the extraction of convincing parameters for diagnosis purpose itself (e.g. for the early detection of deteriorating states of health). Considering the physical shape, the vital capacity VC (depicted in Fig. 2) is a useful score and common in spirometry physicals for the determination of the pulmonary function; an indicator for the physiological performance capability. To interpret the values for the vital capacity VC, depending on the standard breathing volume, the maximum inhaled volume and the maximum exhaled volume, the following Eq. (1) can be used to determine the typical set point for the comparison with measured values. The reference value for the residual volume (remaining air in the lungs) drops from 3–4 L at an age of 20 years to 2 L at an age of 65 years.

$$VC = \frac{height^3}{k} \cdot \left(1.03 - \frac{age - 25}{100} \cdot 0.75\right) \tag{1}$$

with gender factor k

$$k(g) = \begin{cases} 1.0, & g = male \\ 1.1, & g = female \end{cases} \tag{2}$$

Vital capacity	Standard breathing volume	~ 0.5 L
	Inspiration reserve	~1.5-2 L
	Expiration reserve	~1-1.5 L
	Residual volume	~ 3-4 L ~2 L

Fig. 2 Vital capacity

For the continuous approximation of the constituent parts of the vital capacity VC, a previous anthropometric survey including test measurements for system calibration is necessary. This has to be done in accordance to a concomitant body plethysmography. Therefore, features like the thorax and abdomen excursion need to be detected and analyzed in the context of reference measurements. Features of interest are respiratory rate RR, the variability of RR, the amplitude and its variability, significant linear and sometimes exponential trends. These trends can be associated with changes in the residual volume (short-time). That means, the person is breathing erratically. For diagnosis effort, there are also additional features to detect. Most common is the examination of breathing patterns gathered by polysomnographic surveys. Usually, these surveys cover apnoea, hyperpneas or characteristic patterns like Cheyne-Stokes respiration (CSR), Biot's respiration (sometimes called ataxic respiration), Kussmaul breathing and other forms of labored breathing. These phenomena can also be linked to distinct excursion patterns.

Current developments for the detection of breathing parameters can be classified by three main categories: direct measurement of air flow, the measurement of different gas concentrations in the expired air [2] or the blood and finally, the observation of the movement of the thorax or the abdomen or alterations in the tissue impedance. One approach based on the analysis of tri-axial accelerometer data for the detection of breathing rate and flow waveform estimation was proposed by [3]. The extension of this approach deals with the simultaneous monitoring of the activity and the respiration [4]. Also focused on the examination of mechanical signals evoked by the upheaval of the breast, we integrated a sensor component within an armchair and in a bed. Thereby, it is aimed to monitor the patient while he is watching TV, reading a book or executing other activities which can be done in a sitting position. Additionally, the patient can be supervised during the night while he is sleeping.

2 Methodology

The basic concept deals with the investigation of alterations in the UWB-reflection runtime. The concerned reflection is caused by a solid object. In this case, the object is the human body and changes in the body's position or the body's appearance induce also changes in reflection runtime (refer to Fig. 3).

2.1 Related Work

UWB-systems with various types of signal modulation are propagated and tested for diverse applications. In order to discover hidden objects or, in particular humans through massive walls the usage of a *m-sequence radar* was proposed by [5]. Another approach of through-wall radar measurement was introduced by [6]. The assignment of localisation tasks in the context of automobile parking system to

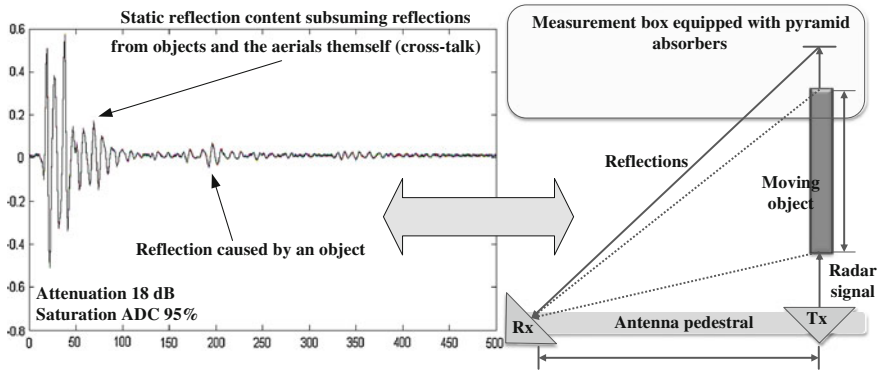


Fig. 3 Working principle

UWB-solutions was proposed by [7]. Much more focusing on aspects of hardware design, [8] presents an on-chip solution with integrated electronics and on-board data processing for UWB radar systems for the detection of humans. Recapitulatory, the elaborate survey about existing through-wall imaging technologies from [9] grants a fruitful overview about the state of the art in this area. Addressing the field of wireless communication, UWB-systems seem to be a promising concept for diverse challenges. Thus, short range communication based on UWB is discussed by [10]. A survey about existing MAC-protocols for ultra-wide-band communication was drafted by [11]. The main objective was the identification of development potentials for an optimal MAC-layer considering the demand for high data rates. [12] proposes a novel methodology for the signal acquisition in UWB-based transmit-only wireless sensor networks. Thereby, the addressed autonomous sensor nodes implement a single code approach to avoid concurrent transmissions and collisions. [13] focusses on the design of filter-antennas for UWB-based communication networks with a bandwidth from 2.65 to 8.52 GHz. An approach for short range communication is proposed by [14] who examines and optimizes the usability of UWB-communication for portable devices. The benefit of UWB-components for BAN-communication in the domain of telemedicine is part of the work of [15]. Concerning our focus of work, UWB-radar was also used to detect vital parameters. In order to correct and calibrate MRI-systems, [16] introduced ultra-wide-band sensing for the detection of the patients exact position regarding imaged body tissue, in particular the chest. The examination of different organic materials in accordance to their content of water is the topic of [17].

2.2 System Setup and Data Processing

For the acquisition of vital signs, an ultra-wide-band radar system, consisting of one transmitting channel and two receiving channels, was embedded within a resting furniture. The connected antennas (type Vivaldi) are installed within the backside of

an armchair and aligned to the abdomen of the sitting person. The armchair provides the advantage that the person sitting inside is tied to a fixed position. This fact is essential; motions of the body exert a disturbing influence on the quality of the reflection pattern because these occurrences are belonging to the same or similar dynamic range as the addressed vital signs. In order to cover a larger body area (possibly to detect heart rate), two sensor systems can be coupled to increase the number of receiving channels up to four. The UWB-system itself modulates a m-sequence of 9th order with a length of 511 samples—the signal energy is equally distributed over a bandwidth $B = f_{max} - f_{min}$ of 3.9 GHz from DC (cut-off -10 dB and a master clock rate of 10.09 GHz. Each sample corresponds to a certain distance resp. expressed by the elapsed propagation time of the signal response. The current sample rate (for a complete frame/scan) is about $0.01496 \text{ s} \leftrightarrow 66.8449 \text{ Hz}$ which is sufficient for the addressed target. For more details about the utilized hardware and the m-sequence modulation refer to [6]. The general procedure for the treatment of the n-dimensional reflection data is depicted in Fig. 4 and starts naturally with the parameterization of the sensor device and the reading of the raw data. A single scan (refer to Fig. 5) leads to a vector

$$X_n = (x_{ij})_{i=1, \dots, 511} = (\text{Sample}_1 \dots \text{Sample}_{511})' \quad (3)$$

with $x_{ij} \in \mathbb{R}$. Unfortunately, due to hardware properties, measurement frames are sometimes mismatching. Hence, it is important to identify a characteristic signal content for adjustment which is present in every single measurement vector of X_n . Referring to the signal curve drawn in Fig. 5, there is an eye-catching signal content marked by the dotted rectangle one. This large polarization marks the reflection caused by the cross-talk of the receiving and transmitting antenna. Knowing the position of both antennas, a point of origin can be determined in order to span a coordinate system. Each vector of index n has to be scaled/shifted to this origin (depends on the reference vector of index r) by the shift factor c_{s_n} .

$$c_{s_n} = \left| \underset{i=1}{\operatorname{argmax}}^{i=511} (|(x_{i1})_n|) - \underset{i=1}{\operatorname{argmax}}^{i=511} (|(x_{i1})_r|) \right| \quad (4)$$

$$X_n^* = (x_{i-c_{s_n}j})_n \quad (5)$$

Now, in accordance to the number of samples Δi between the cross-talk polarization and the object (e.g. marked by the dotted rectangle two), and the spatial resolution Res_s of a single sample, the distance of the object can easily be determined via $d = \Delta i \cdot c \cdot Res_s$. Completing a measurement campaign with the length m (scan) with consecutive scaling, the result is represented by

$$X_c^* = (x_{ij})_{i=1, \dots, 511} \quad (6)$$

$j \dots m$

A graphical representation (of the signal power over time mTs) is illustrated in Fig. 6. Obviously, there are two noticeable regions in the plot—certain, suspicious

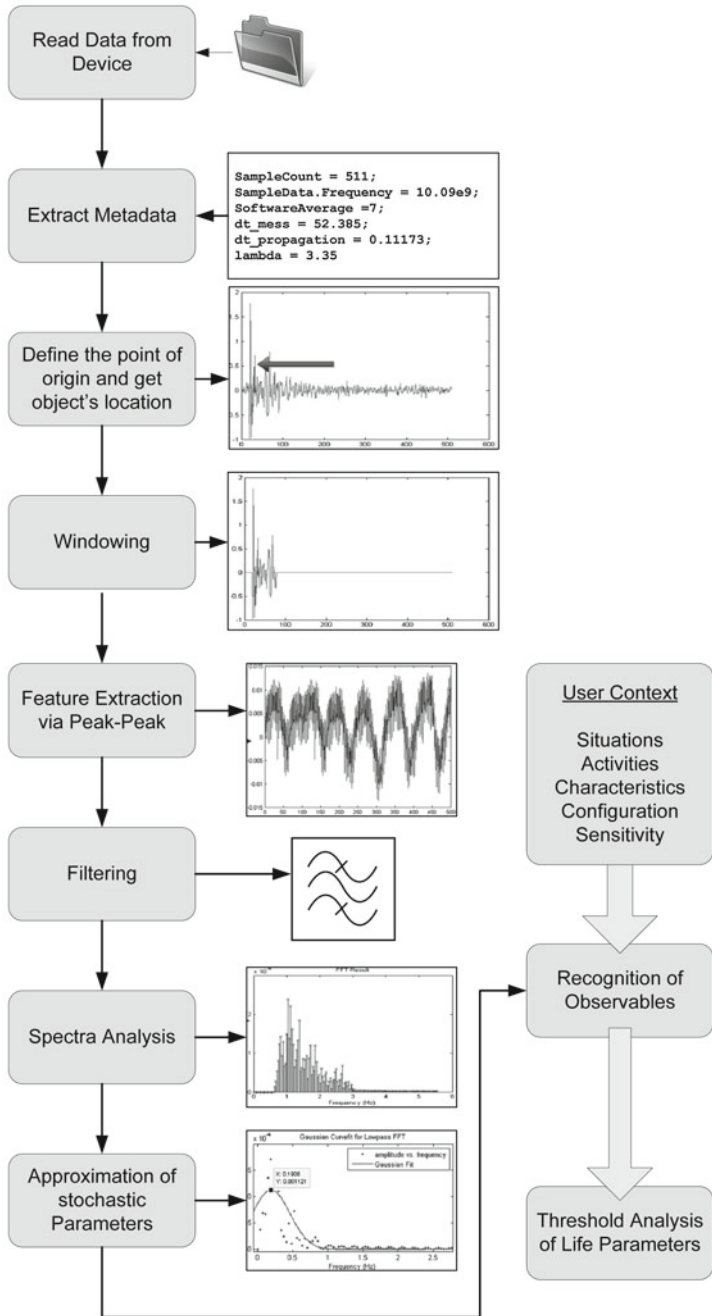


Fig. 4 Process of reflection data analysis

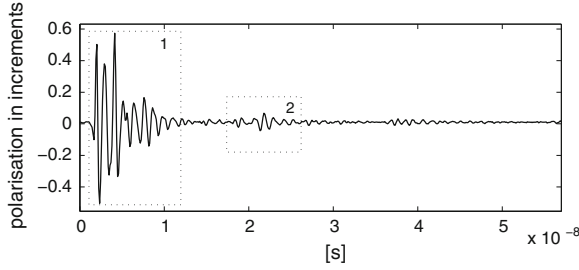


Fig. 5 A single scan with 511 samples

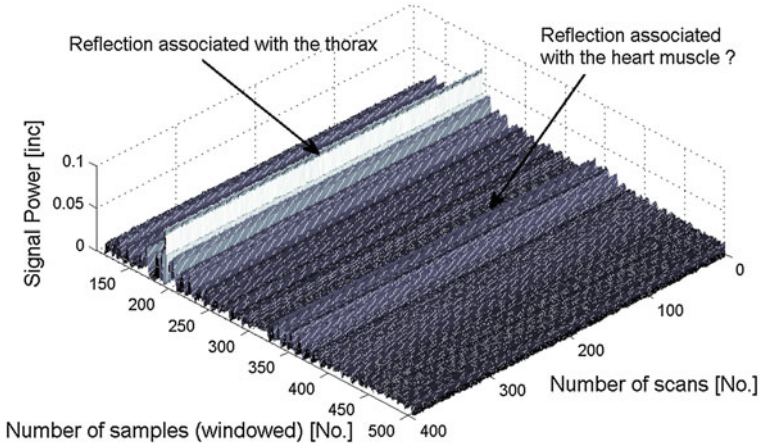


Fig. 6 Temporal behavior of reflections

reflections. These signals may be associated with the cyclic excursion of the thorax and the contraction of the heart muscle. Addressing dynamic processes as the respiratory rate, it is important to consider the static content in the reflection data representing the walls or the furniture in the environment. Therefore, it is important to execute some preliminary measurements X_s^* with a scan length p for the removal of the background. Thus, the underlying dynamic process can be isolated. Due to noise reduction, it is an appropriate method to use the mean vector of $X_s^* = p^{-1}X_s^*1$ for the subtraction.

$$X_d^* = \forall_{i,j}(x_{ij}^* - \bar{x}_{i1}) \quad (7)$$

In order to isolate interesting features within the reflection pattern, data frames X_d^* are parsed for maxima of signal power. Tracking these significant points in data allows the determination of the vertical window size $|w|$.

$$c_m = \underset{i=1}{\operatorname{argmax}}^{i=511}(x_{d_{im}}^*) \quad (8)$$

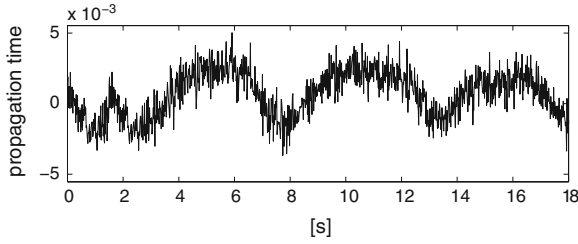


Fig. 7 Extracted movement signal of the first reflection

$$|w| = \max((c_m)) - \min((c_m)) \quad (9)$$

The initial values for the observation window were set in accordance to average amplitude values of breathing. After analyzing the observation window for the first dielectric transient, a timeseries $Y(nTs)$ represented in Fig. 7 is the result.

$$Y(nTs) = T(nTs) + Z(nTs) + S(nTs) + R(nTs) \quad (10)$$

$n \in \mathbb{N}^+, Ts = 0.0149s$

$T(nTs)$ covers the trend in the data, $R(nTs)$ grasps all the noise, and $Z(nTs)$ and $S(nTs)$ represent periodic short- and long-term developments in the signal. A typical reason for an occurring $T(nTs)$ may be a slowly decreasing amplitude in breathing due to emerging edema in the lungs—reciprocal, the frequency might increase. In order to reduce the high content of noise in the signal, filtering with e.g. a moving average is the most common solution. Right at the start, an IIR-filter following the transfer function

$$S(z) = \frac{Y(z)}{X(z)} = \frac{\sum_{k=0}^P b_k z^{-k}}{\sum_{l=0}^Q a_l z^{-l}} \quad (11)$$

$$S(z) = \frac{b_0 + b_1 z^{-1} + b_2 z^{-2} + \dots + b_m z^{-m}}{a_0 + a_1 z^{-1} + a_2 z^{-2} \dots + a_n z^{-n}} \quad (12)$$

was selected to flatten the noise (refer to the filter output drawn in Fig. 8 of the filter input depicted in Fig. 7). Filter coefficients are computed with the aid of

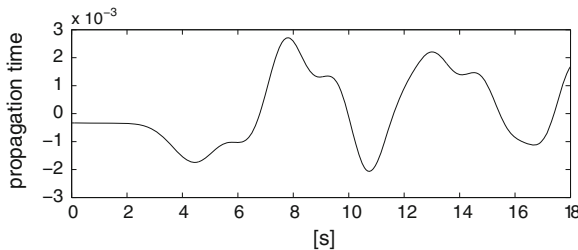


Fig. 8 Response of the IIR-lowpass filter

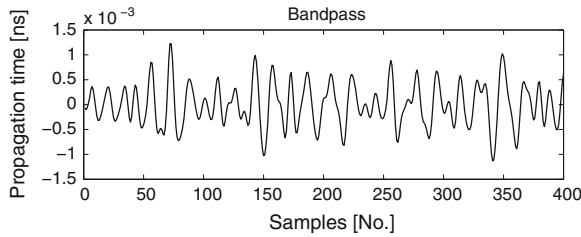


Fig. 9 Response of the IIR-Bandpass filter (heart contraction)

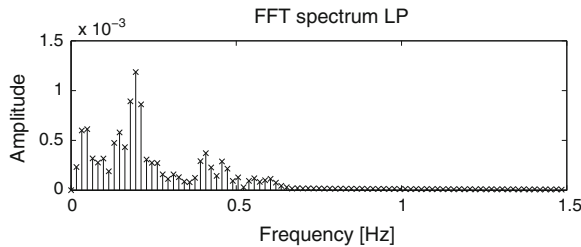


Fig. 10 Spectra of LP-response

Chebyshev-polynomials fitting the demand for an appropriate attenuation regarding a cut-off frequency which corresponds with highest breathing rates. For the isolation of signals with a smaller amplitude and much higher frequencies, a pertinent band-pass filter was designed and implemented (refer to Fig. 9). As expected, filtering the data through an IIR-filter results in a non-linear phase shift of the signal and in an alteration of the underlying curve characteristic. If respiratory rate is the only object of interest, this does not matter; the consecutive windowed FFT-Fast Fourier Transform provides reliable results (refer to Fig. 10). But if it is necessary to identify and localize variances in signal amplitudes or frequencies, and in addition, particular patterns, this filtering procedures deliver timeseries lacking important details of information. Instead of using sinus functions for the decomposition of the timeseries, alternatives of functions only defined over a small interval provide the chance to localize in the time and the frequency domain. Therefore, curve approximation by the superposition of wavelets, an established approach for the compression of data e.g. for pictures, seems to be the best solution to reduce the noise and to preserve important and significant parameters for the feature extraction process. The fundamental idea deals with the approximation of an unknown function f through the superposition

$$f = \sum_k c_k \Psi_k \quad (13)$$

through the basis functions of Ψ_k and the coherent coefficients c_k . The basis functions Ψ_k belong to the orthonormal set of functions $(\Psi_k)_{k \in J}$ with $J \subseteq \mathbb{N}^+$ under the following condition:

$$\langle \Psi_i, \Psi_k \rangle = \delta_{i,k} := \begin{cases} 1, & \text{if } i = k \\ 0, & \text{if } i \neq k \end{cases} \quad (14)$$

That means, the scalar product vanishes. Considering the preferred wavelets, there exist many different types with varying properties. In general, the basis function of Ψ_k is described by

$$\Psi_{c_1, c_2}(t) = \frac{1}{\sqrt{c_1}} \Psi\left(\frac{t - c_2}{c_1}\right), \quad c_1 \in \mathbb{R}^+, c_2 \in \mathbb{R} \quad (15)$$

and called mother wavelet. By varying the parameters c_1, c_2 for the shift and scaling of the wavelet, best fitting coefficients for the approximation of the function f can be derived. Using an recursive procedure, coefficients for a couple of single wavelets for the linear combination can be computed. Thinking about continuous functions of f , the transform is done by

$$CWT(c_1, c_2) = \frac{1}{\sqrt{|a|}} \int_{-\infty}^{+\infty} f(t) \Psi^*\left(\frac{t - c_2}{c_1}\right) \quad (16)$$

For discrete values $f(nTs)$, the Fast Wavelet Transform is used. In order to remove the noise content $R(nTs)$ in the timeseries $Y(nTs)$, the signal was decomposed into the wavelet representations using symlets (modified Daubechies wavelets). After computing the coefficients c_k for the signal reconstruction, the gathered values are modified in accordance to the threshold τ as explained below and used for signal estimation (refer to Fig. 11).

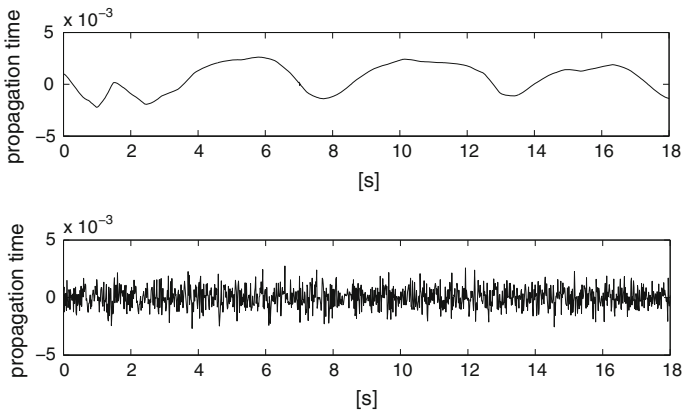


Fig. 11 Denoised signal and separated white noise process

$$c_k = \begin{cases} 0, & c_k \leq \tau \\ c_k, & c_k > \tau \end{cases} \quad (17)$$

This procedure is known as thresholding and realized in two different manners—hard and soft thresholding. Hard thresholding is expressed by the Eq. (17) and means the strict suppression of small coefficients. The alternative soft thresholding deals with shrinkage of the coefficients $c_k \rightarrow \tilde{c}_k$ by the value of τ if c_k is greater than τ .

After retransformation, we get an estimation

$$\tilde{f} = \sum_{k \in J} \tilde{c}_k \Psi_k \quad (18)$$

of the underlying unknown signal of respiratory. Or in other words

$$\tilde{Y}(nTs) = \tilde{Z}(nTs) + \tilde{T}(nTs) + \tilde{S}(nTs) \quad (19)$$

with the separated noise

$$\tilde{R}(nTs) = Y(nTs) - \tilde{Y}(nTs). \quad (20)$$

Figure 12 demonstrates the effect of both techniques. Better results for further considerations are provided by the usage of soft thresholding because the reconstructed signal is much smoother and more often free of any disturbing peaks resp. outliers (refer to the dotted ellipse in Fig. 12). After the removal of the white noise content, the detection of interesting points/areas in the curves was the next issue. Analyzing a couple of reconstructed signals, the detection of extrema sometimes fails due to the movement of the body in the armchair or increasing residual volume—at every intake of breath some additional air remains in the lungs. Assuming,

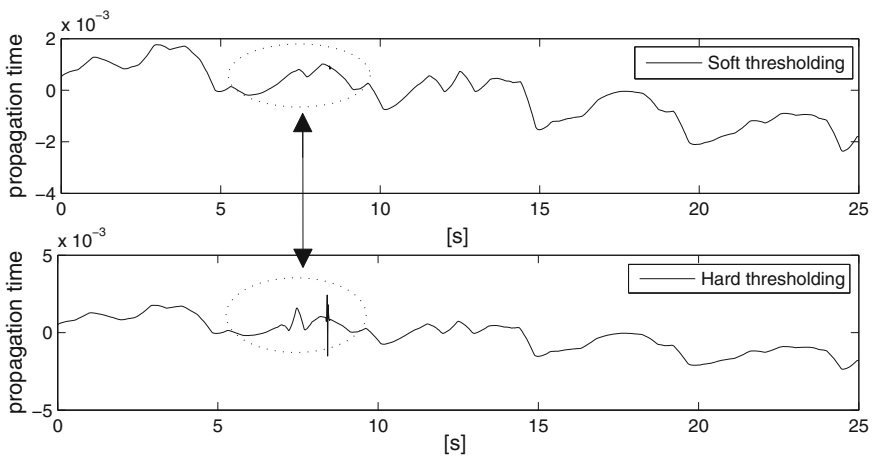


Fig. 12 Hard and soft thresholding of RR-signal

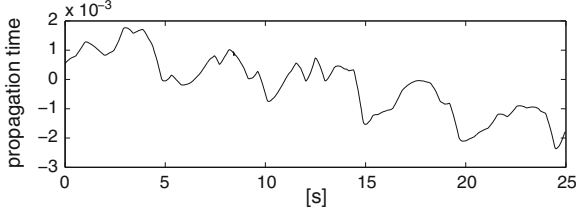


Fig. 13 Breath signal with a decreasing offset

that the reconstructed signal consists of a composition of an indistinguishable long-term seasonal influence ($\tilde{Z}(nTs) \rightarrow 0$), some variously weighted trend functions

$$\tilde{T}(nTs) = \sum_{i=1}^{i=\infty} f_i(nTs), \quad (21)$$

and the sought-after hidden process $\tilde{S}(nTs)$, covering the short-time periodic behavior, it is useful to remove disturbing components for the segmentation of the series in the time domain. Using a model reduced to a linear trend and, in accordance to previous observations, some exponential or power behavior, we obtain

$$\tilde{Y}(nTs) = \tilde{S}(nTs) + \tilde{T}(nTs) \quad (22)$$

with a set of basic functions after the removal of the steady component $c_1nTs + c_2$ in the signal (refer to the example in Fig. 13).

$$f_{T1}(nTs) = c_1e^{c_2nTs} \quad (23)$$

$$f_{T2}(nTs) = c_3e^{c_4nTs} + c_5e^{c_6nTs} \quad (24)$$

$$f_{T3} = c_7e^{\frac{nTs-c_8}{c_9}} \quad (25)$$

$$f_{T4} = c_{10}nTs^{c_{11}} + c_{12} \quad (26)$$

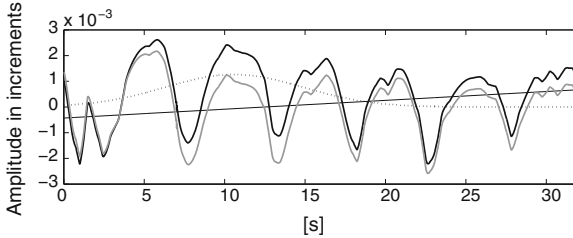


Fig. 14 Decomposition of the extracted RR-signal

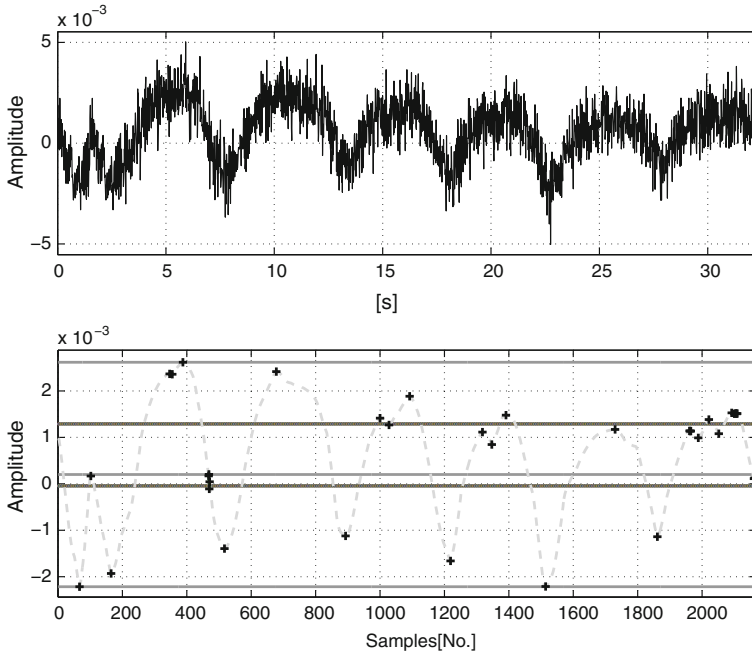


Fig. 15 Significant points in the RR-signal

For the approximation of the influence induced by the movement or motion of the body, coefficients c_i for the mentioned relationships are interpolated. The best fitting function f_{Tr} for the trend removal is selected due to

$$f_{Tr}, r = \underset{i=1}{\overset{i=4}{\operatorname{argmin}}} (SSE_i). \quad (27)$$

After the abatement of these components (refer to Fig. 14 with the different trend components of the extracted RR-signal), significant points as extrema are ascertained via interval evaluation. Examining the rectified series, significant extrema are detected. Of course, there are accumulations of these points in relation to the degree of remaining noise or peaks and obviously, to the characteristics of the breathing process itself (ref to Fig. 15). Due to their nearby unique occurrence (in comparison to the high points), the low points of the curve are helpful for the partition of the data to smaller evaluation intervals. Assuming that the largest value in each interval marks the end of each single breathing process (end of inhalation), these points are selected for the computation of frequency, and after rescaling (adding previously removed non-linear trend) of the timeseries, the breathing amplitude. Additionally, the low points are checked due to their Euclidean distance; if it seems that they belong together, a surrogate low point is computed and used for the interval limitation. Furthermore, each identified extrema is weighted

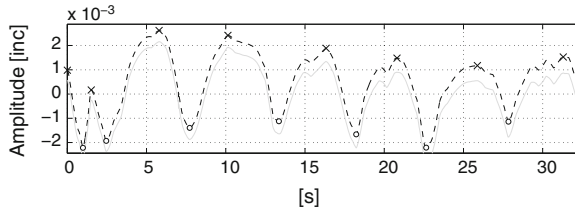


Fig. 16 Selected extrema in respiratory pattern

due to its location within the σ -bounds of the distribution describing the general stochastic signal properties considering a sensitivity factor c_s . In summary, the process ends with the provision of RR, RRV, AR, ARV and in addition, with the localization of leaps and existing non-linearity within the data. These observations need to be matched to distinct patterns as mentioned in section 2.B (Fig. 16).

3 Discussion of Results

In the early stages of research, preliminary measurements with deterministic signal sources were executed. A programmable linear motor was configured to perform motions with specified values for acceleration, velocity and distance. The maximum periodic displacement of the armature of 45 cm was detected with an exact match of 99.97 %. The lowest possible motion of the drive of 1 mm was detected with an accuracy of 99.6 %; a fine result for further considerations. That means, it was not possible to determine the best resolution because the drive itself is limited to 1 mm movement range.

Considering respiratory rate and variances in frequency and amplitude, the main target of unobtrusive vital sign acquisition via UWB was accomplished. After improving the hardware setup through auxiliary shielding in the backside of the armchair, an increased robustness against disturbing backscattering was achieved. In relation to our reference measurement device, a pulse oximeter with nasal prongs (of course, observed signals are phase shifted, but have the same properties) a sufficient accuracy was reached (refer to Table 1). In addition, the accuracy and

Table 1 Results of RR-measurement-FFT based

Test person	Accuracy (respiratory rate %)	Accuracy respiratory rate (shielded %)
Male, 1.84 m, 74 kg	86	91.5
Male, 1.72 m, 82 kg	87	92.1
Male, 1.92 m, 79 kg	84	92.4
Male, 1.81 m, 76 kg	87	91.6
Female, 1.67 m, 59 kg	71	91.2
Average values	83	91.7

Table 2 Results of RR-measurement—FWT-based

Test person	Accuracy (respiratory rate %)	Accuracy respiratory rate variability (%)
Male, 1.84 m, 74 kg	95.4	67.5
Male, 1.72 m, 82 kg	96.3	72.1
Male, 1.92 m, 79 kg	95.2	69.4
Male, 1.81 m, 76 kg	97.2	69.6
Female, 1.67 m, 59 kg	94.7	68.2
Average values	95.7	69.3

robustness for long-term measurement was improved by the evaluation of different antenna topologies and their recalibration (direction and position). The accuracy of RR-detection indexed by a was determined by measurement campaigns without the mentioned hardware improvement. For the feature extraction in both campaigns, a FFT with a consecutive spectrum distribution analysis was executed. Obviously, the measurement accuracy depends on the constitution of the test person. Thinking about heart rate detection, which is also part of our work, there are still open issues. Accuracy for the detection of signals in this range drops to 43 % in comparison to the accuracy of the RR-detection. The denoising of signals by wavelets including a consecutive analysis in the time domain arose as a convenient alternative; the accuracy of measurement of RR and its features rose significantly (refer to Table 2). The amplitude of the respiratory signal was measured with an accuracy of 86.4 %. Possibly, an optimization of trend approximation can improve this result. The variance of this feature lacks accuracy and stays at 56 % in comparison to the reference system.

In summary, the results in Tables 1 and 2 show the benefit of analysis of the extracted signals in the time domain. FWT-based denoising is the better approach for filtering, because interesting features in the signal are preserved. In addition, suspicious patterns are easier to recognize which is an important insight for the next steps.

4 Conclusion and Outlook

As shown in the previous sections, the current state of research demonstrates the potential benefit for the unobtrusive acquisition of vital signs which are incidental to mechanical measures. Especially in the domain of geriatric care, according to specific user demands, this approach seems to be worthwhile for practical application. Not only restricted to home care scenarios or applications of Ambient Assisted Living, this technical solution can, embedded within information processing infrastructures, improve the accuracy of situation recognition systems and additionally raise the diagnostic efficiency of such approaches. Thinking about stand-alone solutions, this work can be the springboard for the development of a

new type of telemedical devices—the fusion of furniture with ambient intelligence focusing on health monitoring. At the present time, the work concentrates on the detection and collating of respiratory patterns. At the beginning of September 2012, clinical trials with different objectives will start. After examining and improving the robustness and accuracy of proposed approach in daily use for the detection of respiratory rate and related features (patterns also), it is aimed to detect the heart rate and arrhythmias in a reliable manner. In addition, it is planned to aggregate ECG-recordings of atrial fibrillation with reflection patterns in order to identify correlations between mechanical and bioelectrical observations assigned to the same signal source. Furthermore, it is scheduled to perform test campaigns with patients with congestive heart failure in order to detect edema in the lungs by the evaluation of the thorax impedance. Current test measurements in our laboratory with a mock-up prove the meaningfulness of the implemented general functional principle but it is necessary to confirm it for practice by examining persons with altering fluid retentions considering calibrated reference measuring. And finally, derived vital sign must be assessed in the light of the user situation or user activity.

References

1. Busch, B.H., Kujath, A., Withoef, H., Welge, R.: Preventive emergency detection based on the probabilistic evaluation of distributed, embedded sensor networks. In: *Ambient Assisted Living*. Springer, Berlin (2011)
2. Folke, M., Cernerud, L., Ekstroem, M., Hoek, B.: Critical review of non-invasive respiratory monitoring in medical care. *Med. Biol. Eng. Comput.* **41**, 377–383 (2003)
3. Bates, A., Ling, M., Mann, J., Arvind, D.K.: Respiratory rate and flow waveform estimation from tri-axial accelerometer data. In: *Proceedings of International Body Sensor Networks (BSN) Conference*, pp. 144–150 (2010)
4. Mann, J., Rabinovich, R., Bates, A., Giavedoni, S., MacNee, W., Arvind, D.K.: Simultaneous activity and respiratory monitoring using an accelerometer. In: *Proceedings of the International Body Sensor Networks (BSN) Conference*, pp. 139–143 (2011)
5. Sachs, J., Friedrich, J., Zetik, R., Peyerl, P., Klukas, R., Crabbe, S.: Through-wall radar. In: *Proceedings of the IRS (2005)*
6. Judson Braga, A., Camillo, G.: An ultra-wideband radar system for through-the-wall imaging using a mobile robot. In: *Proceedings of the ICC'09—IEEE International Conference on Communications (2009)*
7. Mary, g.i., Prithiviraj, v.: Improved UWB localization technique for precision automobile parking system. In: *Proceedings of the TENCON 2008—2008 IEEE Region 10 Conference (2008)*
8. Chang, S., Chu, T.S., Roderick, J., Du, C., Mercer, T., Burdick, J.W., Hashemi, H.: UWB human detection radar system: A RF CMOS chip and algorithm integrated sensor. In: *Proceedings of the IEEE International Ultra-Wideband (ICUWB) Conference*, pp. 355–359 (2011)
9. Michal, A.: Through wall imaging with UWB radar system. Dissertation, Faculty of Electrical Engineering and Informatics, Department of Electronics and Multimedia Communications (2009)

10. Ahmadian, Z., Shenouda, M.B., Lampe, L.: Design of pre-rake DS-UWB downlink with pre-equalization. *IEEE J. Commun.* **40**, 400–410 (2012)
11. Zin, M. S. I. M., Hope, M.: A review of UWB MAC protocols. In: Proceedings of 6th Advanced International Telecommunications (AICT) Conference, pp. 526–534 (2010)
12. Li, Z., Gielen, G.: UWB signal acquisition in transmit-only networks. In: Proceedings of IEEE International Ultra-Wideband (ICUWB) Conference, pp. 126–129 (2011)
13. Panda, J. R., Kakumanu, P., Kshetrimayum, R.S.: A wide-band monopole antenna in combination with a UWB microwave band-pass filter for application in UWB communication system. In: Proceedings of Annual IEEE India Conference (INDICON), pp. 1–4 (2010)
14. Xiao, Z., Ge, N., Pei, Y., Jin, D.: SC-UWB: a low-complexity UWB technology for portable devices. In: Proceedings of IEEE International Signal Processing, Communications and Computing (ICSPCC) Conference, pp. 1–6 (2011)
15. Hernandez, M., Kohno, R.: UWB systems for body area networks in IEEE 802.15.6. In: Proceedings of IEEE International Ultra-Wideband (ICUWB) Conference, pp. 235–239 (2011)
16. Thiel, F., Hein, M., Schwarz, U., Sachs, J., Seifert, F.: Combining magnetic resonance imaging and ultra-wideband radar: a new concept for multimodal biomedical imaging. In: *Rev Sci Inst* **80**, 014302 (2009)
17. Marko H., Jrgen S., Ulrich S., Schaefer, M.: Ultrabreitband-Sensorik in der medizinischen Diagnostik, In: 41. Jahrestagung der Deutschen Gesellschaft fuer Biomedizinische Technik BMT, Aachen, Germany (2007)